

Submitted to: JCAP

X-ray photons from late-decaying majoron dark matter

Federica Bazzocchi¹, Massimiliano Lattanzi², Signe Riemer-Sørensen³ and Jose W. F. Valle¹

¹ AHEP Group, Institut de Física Corpuscular (C.S.I.C./Universitat de Valencia) Edifici Institutos de Paterna, Apt 22085, E-46071 Valencia, Spain

² Oxford Astrophysics, Denis Wilkinson Building, Keble Road, OX1 3RH, Oxford, UK and Istituto Nazionale di Fisica Nucleare, Via Enrico Fermi 40, 00044 Frascati (Rome), Italy

³ Dark Cosmology Centre, Niels Bohr Institute, University of Copenhagen, Juliane Maries Vej 30, DK-2100 Copenhagen, Denmark

E-mail: fbazzo@ific.uv.es

E-mail: mxl@astro.ox.ac.uk

E-mail: signe@dark-cosmology.dk

E-mail: valle@ific.uv.es

PACS numbers: 14.60.Pq, 12.60.Jv, 14.80.Cp

Abstract.

An attractive way to generate neutrino masses as required to account for current neutrino oscillation data involves the spontaneous breaking of lepton number. The resulting majoron may pick up a mass due to gravity. If its mass lies in the kilovolt scale, the majoron can play the role of late-decaying Dark Matter (LDDM), decaying mainly to neutrinos. In general the majoron has also a sub-dominant decay to two photons leading to a mono-energetic emission line which can be used as a test of the LDDM scenario. We compare expected photon emission rates with observations in order to obtain model independent restrictions on the relevant parameters. We also illustrate the resulting sensitivities within an explicit seesaw realisation, where the majoron couples to photons due to the presence of a Higgs triplet.

1. Introduction

While solar and atmospheric neutrino experiments [1, 2, 3] are confirmed by recent data from reactors [4] and accelerators [5] indicating unambiguously that neutrinos oscillate and have mass [6], current limits on the absolute neutrino mass scale,

$$m_\nu < 1 \text{ eV} \quad (1)$$

that follow from beta [7] and double beta decay studies [8], together with cosmological observations of the cosmic microwave background (CMB) and large scale structure [9] preclude neutrinos from playing a direct role as dark matter.

However, the mechanism of neutrino mass generation may provide the clue to the origin and nature of dark matter. The point is that it is not unlikely that neutrinos get their mass through spontaneous breaking of ungauged lepton number [10, 11]. In this case one expects that, due to non-perturbative quantum gravity effects that explicitly break global symmetries [12], the associated pseudoscalar Nambu-Goldstone boson – the majoron J – will pick up a mass, which we assume to be at the kilovolt scale [13]. The gauge singlet majorons resulting from the associated spontaneous L -violation will decay, with a very small decay rate, mainly to neutrinos. However, the smallness of neutrino masses (Eq. (1)) implies that its couplings to neutrinos g_J are rather tiny and hence its mean life is extremely long, typically longer than the age of the Universe. As a result such majorons can provide a substantial fraction, possibly all, of the observed cosmological dark matter.

Here we show how the late-decaying majoron dark matter (LDDM) scenario, and in particular the majoron couplings g_J and g_γ to neutrino and photons respectively, can be constrained by cosmological and astrophysical observations.

The paper is organized as follows. In Sec. 2 we describe the basic cosmological constraints on the LDDM scenario, in Sec. 3 we describe the “indirect detection” of the LDDM scenario and determine the restrictions on the relevant parameters that follow from the x-ray background and the emission from dark matter dominated regions. In Sec. 4 we compare the sensitivities of CMB and x-ray observations to the LDDM scenario, stressing the importance of the parameter $R = g_J/g_\gamma$. Finally in Sec. 5 we discuss an explicit seesaw model realisation of the LDDM scenario, where the majoron couples to photons due to the presence of a Higgs triplet.

2. Cosmological constraints

The LDDM hypothesis can be probed through the study of the CMB anisotropy spectrum. In fact, current observations, mainly of the Wilkinson Microwave Anisotropy Probe (WMAP) lead to important restrictions. Indeed, the LDDM scenario has been explored in detail within a modified Λ CDM cosmological model; in particular, it has been shown that the CMB anisotropies can be used to constrain the lifetime $\tau_J = \Gamma_J^{-1}$ and the present density $\Omega_J = \rho_J/\rho_c$ of the majoron [15].

The reason is that the late decay of majorons to neutrinos would produce too much power at large scales, through the late integrated Sachs-Wolfe effect, thus spoiling the CMB anisotropy spectrum. WMAP third year data [14] can be used to constrain:

$$\tau_J < 1.3 \cdot 10^{19} \text{ sec}^{-1}; \quad (2)$$

at 95% CL [15].

This result is independent of the exact value of the decaying dark matter particle mass, and is quite general, in the sense that a similar bound applies to all invisible decays of cold or warm dark matter particles [16, 17, 18].

The CMB spectrum can also be used to constrain the majoron energy density. This can be translated to a limit on the majoron mass in a model-dependent way. Given the majoron mass m_J and lifetime τ_J , the present majoron density parameter Ω_J can be written as:

$$\Omega_J h^2 = \frac{m_J}{1.25 \text{ keV}} e^{-t_0/\tau_J}; \quad (3)$$

where h is the dimensionless Hubble constant, t_0 is the present age of the Universe, and the parameter Ω_J encodes our ignorance about the number density of majorons. The normalization in Eq. 3 is chosen such that $\Omega_J = 1$ if (i) the majoron was in thermal equilibrium in the early Universe; and (ii), it decoupled sufficiently early, when all the quantum degrees of freedom in the standard model of fundamental interactions were excited.

This simple picture can be changed if: (i) The majoron could not thermalize before it decoupled from the other species, or (ii) The entropy generated by the annihilation of some particle beyond the standard model diluted the majoron abundance after its decoupling.

In any case it is reasonable to assume that the majoron decoupled at $T \lesssim 170 \text{ GeV}$ since its couplings to all the other particles in the standard model (SM) are tiny. Using the WMAP third year data, the following constraint on $\Omega_J h^2$ can be obtained (95% C.L.) assuming the dark matter to consist only of majorons [15]:

$$0.09 < \Omega_J h^2 < 0.13 \quad (4)$$

Since Eq. (2) implies $\tau_J > t_0$, the above constraint together with Eq. (3) gives:

$$0.12 \text{ keV} < m_J < 0.17 \text{ keV} \quad (5)$$

Our ignorance of the details of the majoron production mechanism, namely the value of λ , can always be used in order to accommodate additional restrictions to the majoron mass m_J coming from observations of the large scale structures.

The limits quoted above apply to the invisible decay $J \rightarrow \nu \bar{\nu}$. There exist also the very interesting possibility to use the CMB polarization to directly constrain the radiative decay $J \rightarrow \gamma \gamma$. This is because photons produced by dark matter decay can inject energy into the baryonic gas and thus affect its ionization history. This will ultimately lead to modifications of the CMB temperature-polarization (TE) cross-correlation and polarization auto-correlation (EE) power spectra. In Ref. [19], WMAP

third year data are used to obtain the following constraint for the radiative decay width Γ_{rad} of long lived dark matter particles like the majoron:

$$\Gamma_{\text{rad}} < 2.4 \times 10^{25} \text{ sec}^{-1}; \quad (6)$$

where η is an "efficiency" factor describing the fraction of the decay energy actually deposited in the baryon gas. This depends, among other things, on the energy of the emitted photon. As a rule of thumb, consider that for redshifts $10 < z < 1000$, when most of the hydrogen is neutral, photons with energy in the range 13.6 eV (the hydrogen ionization threshold) to approximately 1 keV will transfer most of their energy to the baryon gas through photo-ionizations, so $\eta \approx 1$. On the other hand, the Universe is transparent with respect to the propagation of photons with $E > 1 \text{ keV}$, and in this energy range one expects to have $\eta \approx 0$ and then no significant upper limit on Γ_{rad} can be obtained from CMB polarization.

3. X-ray analysis

In a variety of neutrino mass generation models with spontaneous violation of lepton number, majorons have an effective interaction term with photons

$$g_J J F F : \quad (7)$$

Majorons in the keV range are therefore expected also to decay radiatively into two photons of energy $E = m_J/2$, since the decay can be considered to a very good approximation as happening in the dark matter rest frame. This leads to a mono-energetic emission line as a characteristic signal of our decaying dark matter model.

Such an emission line could be possibly be detected both in the diffuse x-ray background and in the emission from dark matter dominated regions. We now consider the constraints coming from both kinds of observations.

In the following, when necessary, we will consider a LDDM scenario within a Λ CDM cosmology with $\Omega_{\text{DM}} = 0.75$, $\Omega_{\text{DM}} h^2 = 0.11$, $\Omega_{\text{b}} h^2 = 0.022$, and $h = 0.72$, corresponding to the best fit values of the CMB analysis in Ref. [15].

3.1. Diffuse x-ray background

Photons produced in late majoron decays will show up in the diffuse x-ray background, if the Universe is transparent with respect to their propagation. This is indeed the case after the Universe has been completely reionized ($z \lesssim 10$): photo-ionization is no more effective in absorbing the photon energy, simply because there are no more neutral hydrogen atoms to be ionized.

The flux $F(E)$ of decay radiation at the present time ($z = 0$) is given by [20]:

$$F(E) = \frac{c}{4} \frac{E}{E_0} \frac{N_J n_J(z)}{H(z)} \quad (8)$$

$1+z=E_0/E$

where $N = 2$ is the number of photons produced in each decay, $n_J(z)$ is the number density of majorons at redshift z , $H(z)$ is the Hubble parameter, and $E_0 = m_J/2$ is

the energy of the photons produced in the decay. This can differ from the energy E at which we are observing due to the cosmological redshift of photons. In other words, when looking today at an energy $E < m_J/2$ we can still expect some signal from photons emitted in the past with energy $E = m_J/2$ that have been red-shifted to lower energies.

However we know from the CMB that the majoron is very long lived, so that we expect the decay spectrum to be dominated by very recent decays. We model the spectrum as mono-energetic with $E = E_0$ and a flux given by:

$$F(E) = \frac{c N_J n_{0,J}}{4 H_0}; \quad (9)$$

where the subscript 0 denotes quantities evaluated at the present time.

This should be compared with the observed diffuse x-ray flux from ASCA [21] and HEAO-1 [22], operating in the 0.4-7 keV and 3-500 keV ranges respectively. The flux can be modeled as [23] (units are $\text{sec}^{-1} \text{cm}^{-2} \text{sr}^{-1}$):

$$F_{\text{obs}}(E) = \begin{cases} 8 \frac{E}{\text{keV}}^{0.4}; & 1 \text{ keV} < E < 25 \text{ keV}; \\ 380 \frac{E}{\text{keV}}^{1.6}; & 25 \text{ keV} < E < 350 \text{ keV}; \\ 2 \frac{E}{\text{keV}}^{0.7}; & 350 \text{ keV} < E < 500 \text{ keV}; \end{cases} \quad (10)$$

Below 1 keV, the strong galactic emission must be carefully removed in order to find the extragalactic signal [24], and consequently we do not extrapolate the above approximation to lower energy for the purpose of the present analysis.

Then, requiring $F(E) = F_{\text{obs}}$ yields an upper limit for the majoron decay width to two photons Γ_J . In particular, in the range, $1 \text{ keV} < E < 25 \text{ keV}$ we have:

$$\frac{\Gamma_J}{\text{sec}^{-1}} \leq 4.45 \cdot 10^{27} \frac{h}{0.72} \frac{\Gamma_J h^2}{0.11} \frac{m_J}{\text{keV}}^{0.6}; \quad (11)$$

This limit, together with the constraints at higher energies, is shown in Fig. 1.

This simple analysis, and the resulting constraint, can be improved in two ways. First of all, one can look for small distortions in the smooth diffuse flux produced by a DM emission line that is possibly lying well below the background signal. In addition, one can take into account the contribution to the signal coming from the Milky Way. This was applied to the HEAO-1 data in Refs. [25, 26]; in this way, the above constraints can be improved by as much as three orders of magnitude (see below). Finally, we note that bounds in the soft x-ray region can be obtained from the observations of a high-resolution spectrometer [27].

3.2. X-rays from dark matter dominated regions

Observations of the x-ray emission from dark matter dominated regions can be used to restrict the decay rate into photons and the mass of any dark matter candidate with

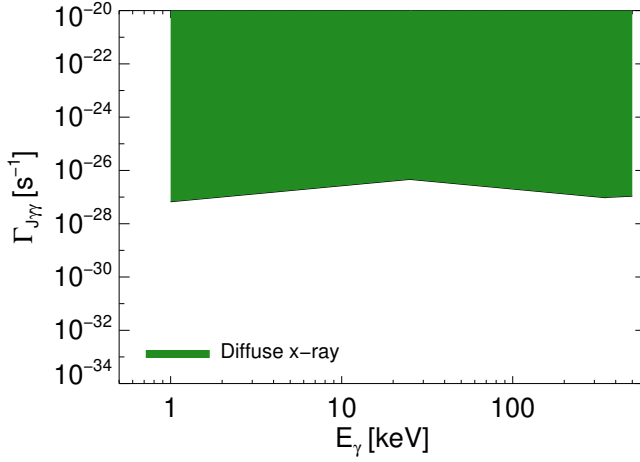


Figure 1. Upper limit from the diffuse x-ray argument. The filled region is excluded. Data from [21, 22].

a radiative two-body decay. This follows from the consideration that the detected flux from a dark matter dominated object gives a very conservative upper limit on the flux generated by dark matter decays in that object.

Since the dark matter in cosmological structures is practically at rest ($v/c \sim 10^{-4}$), the line broadening due to motion of the dark matter is negligible compared to the instrumental resolution of current day x-ray detectors. Hence, a good instrumental spectral resolution increases the sensitivity to a mono-energetic emission line.

Formajrons the 0.1-0.3 keV x-ray interval is very interesting. Unfortunately this range is not accessible with any of the standard CCD instruments on board the present x-ray observatories Chandra and XMM-Newton. However, Chandra carries the High Resolution Camera (HRC) which combined with the Low Energy Transmission Grating (LETG) makes it possible to obtain spectra in the 0.07-10.0 keV range. The resolution of grating spectra is very high ($E_{FWHM} \sim 1$ eV) [28] but all spatial information about the photon is lost, except that it is known to origin from within the field of view (apart from minor effects of scattering along the line of sight).

To reach the maximum resolution requires bright point like sources located at the aim point of the observation. Unfortunately dark matter structures have spatially extended distributions and will produce a very faint signal, if any. Extended sources can be thought of as made up of many point sources, but then most of the sources are off-axis. The effect of a source being off-axis is, that in the detector plane, there is an ambiguity between angle and photon energy, which gives a "smearing" towards lower energies and hence a line broadening in the obtained spectra. The line smearing is energy dependent and worst for high energies [29].

No optimal sources for a search for dark matter decay line emission have been observed with HRC/LETG. Still, from grating observations of an active galaxy, we have improved the upper limit on the decay rate from the dark matter halo in which the

active galactic nuclei is embedded by orders of magnitude. For photon energies above 0.3 keV better constraints are obtained from conventional x-ray CCD observations of merging clusters of galaxies such as the Bullet Cluster [30] or Abell 520 [29].

We have studied a Chandra HRC/LETG observation of the Seyfert 1 galaxy NGC 3227 (observation id 1591), shown in Fig. 2. NGC 3227 has a redshift of $z = 0.004$, which corresponds to a luminosity distance of 16.7 Mpc. The data has been processed and analysed with CIAO version 3.4 using CALDB version 3.4.0 [31]. The obtained spectrum is shown in Fig. 2.

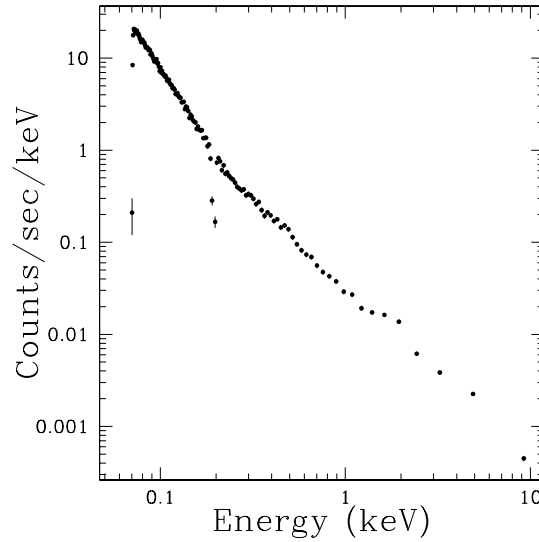


Figure 2. The observed Chandra HRC/LETG spectrum of NGC 3227 (folded with the instrumental response).

In general, the instrumental response cannot be unfolded from the spectrum in a model independent way. Instead a model is folded with the instrumental response and fitted to the data using χ^2 statistics (here we have used the spectral fitting package Sherpa distributed with CIAO).

The model is used to determine an upper limit on the received flux. Since no physical quantities are derived from the empirical model, it is chosen to fit the data (and as such do not necessarily represent a physical model of the emission). The data were split into two intervals: 0.072-0.276 keV and 0.276-4.14 keV and fitted separately to models composed of a power law and four Gaussians for the lower interval and two power laws and two Gaussians for the higher interval. In order to ensure that no emission lines are sticking above the model, the fitted model was re-normalised so there were no bins in the spectrum at more than 2 σ above the model.

As mentioned above, any emission line is smeared out because of the instrumental resolution. Towards lower energies the smearing has the shape of a Gaussian with the width given by the instrumental resolution. Towards higher energies, where the extension of the source plays a role, the smearing depends on the overall distribution

of the dark matter. We have assumed an Navarro, Frenk & White (NFW) [32] profile for the dark matter halo of NGC 3227 with a scale radius of 15 kpc and a virial radius of 200 kpc. These are conservative representative values for galaxies, in the sense that most galaxies have a smaller scale radius and a smaller radius, leading to less smearing (and thereby tighter constraints). The resolution is only sensitive to the full width at half maximum of the density profile, so that choosing a different parameterization (e.g. Moore [33]) would not significantly alter the results.

Since we are only interested in the upper limit on the measured flux, it has been determined in slices of width $E + \text{FWHM}_{\text{instrumental}} > E > E - \text{FWHM}_{\text{smearing}}$ instead of the exact shape of the smeared lines (the difference between the two methods is negligible [29]).

The mass of NGC 3227 has been taken to be 10^{11} solar masses which is conservatively low based on the luminosity of the galaxy [34]. The observational field of view is 25 kpc at the distance of NGC 3227, reducing the observed mass to about a tenth of the total mass. This is probably an underestimate of the observed mass, but a larger observed mass will only improve the constraints.

Assuming only one kind of dark matter, the observed flux, F_{obs} , at a given photon energy yields an upper limit on the decay rate from two-body radiatively decaying dark matter:

$$J < \frac{8 F_{\text{obs}} D_L^2}{M_{\text{fov}}} : \quad (12)$$

The determined flux is dominated by the baryonic emission of the galaxy, which varies with energy, introducing an apparent energy dependence on the constraint.

The resulting constraint on the decay rate is shown in Fig. 3 together with earlier published constraints.

4. X-ray versus CMB

In the previous sections we have shown how the CMB can be used to constrain the invisible decay $J \rightarrow \nu \bar{\nu}$, while x-ray observations can constrain the radiative decay $J \rightarrow \gamma z$. From a theoretical point of view, a very important quantity is the branching ratio of the decay into photons $\text{BR}(J \rightarrow \gamma z)$ that, as long as the decay to neutrinos is by far the dominant channel, is given by the ratio of the decay widths:

$$\text{BR}(J \rightarrow \gamma z) \equiv R = \frac{\Gamma_{\gamma z}}{\Gamma_{\nu \bar{\nu}}} : \quad (13)$$

Note that the decay $J \rightarrow \nu \bar{\nu}$ arises at the tree-level, while the radiative $J \rightarrow \gamma z$ mode proceeds only through a calculable loop diagram. Beyond this, theory can not predict the expected value of R , which is strongly model-dependent. Here we use R as a

we do not consider the CMB polarization limit in the following because (i) it depends on the efficiency of the energy transfer to the baryonic gas and (ii) it turns out to be less constraining than x-rays in the regions of interest.

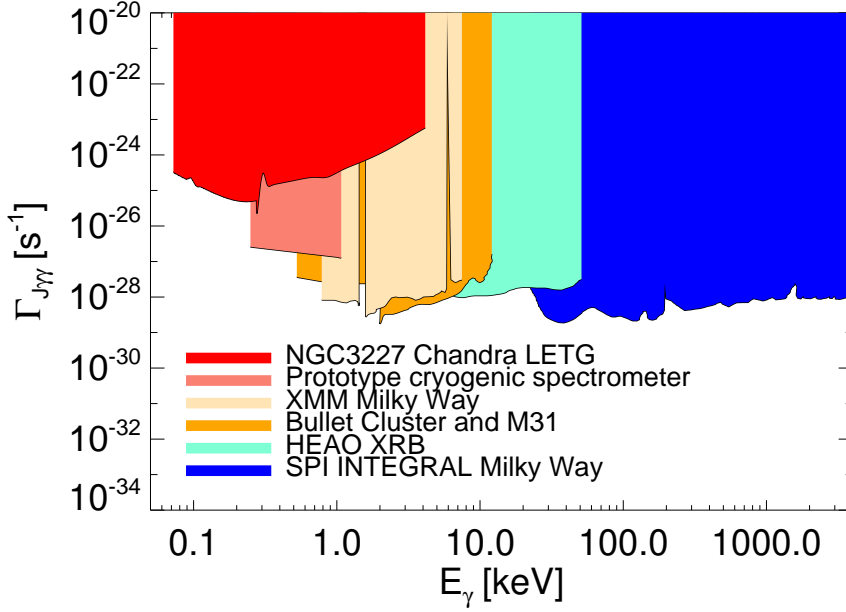


Figure 3. Upper limit on the decay rate from NGC 3227 (red), the Milky Way halo observed with a prototype cryogenic spectrometer (salmon) [27], XMM observations of the Milky Way (sand) [35], Chandra observations of the Bullet Cluster [30] and M31 [36, 37] (orange), HEAO-1 observations of the diffuse x-ray background (aquamarine) [25, 26], INTEGRAL SPI line search in the Milky Way halo (blue) [38, 39]. Filled regions are excluded.

phenomenological parameter varying over the wide range $10^{-25} - 10^{-3}$ (see, for instance, Fig. 6 below). It should be clear that the observations described in Secs. 2 and 3 restrict Γ_γ and Γ_γ , leaving the branching ratio unconstrained.

However, we are also interested in knowing for which models the x-ray observations can probe the decaying majoron dark matter hypothesis with higher sensitivity than the CMB. In particular, we expect that models with large branching ratios will be better constrained by the x-ray observations, since they will predict a larger production of photons.

The x-ray limits presented in Sec. 3 have a mass dependence, which we need to take into account in our assessment of the relative constraining power of the two types of observations. We know, however, from the CMB (see Eq. 5) that:

$$\frac{0.12 \text{ keV}}{m_J} \sim \frac{0.17 \text{ keV}}{m_J}; \quad (14)$$

at 95% C.L. Fixing the value of Γ_γ is then equivalent to fixing the majoron mass, apart from a small uncertainty (which we take into account, see below). We express our result in terms of Γ_γ instead than m_J .

In order to compare the CMB and the x-ray constraints, we fix the value of Γ_γ and determine the corresponding observational ratio of $\Gamma_\gamma = \Gamma_\gamma$. According to the CMB

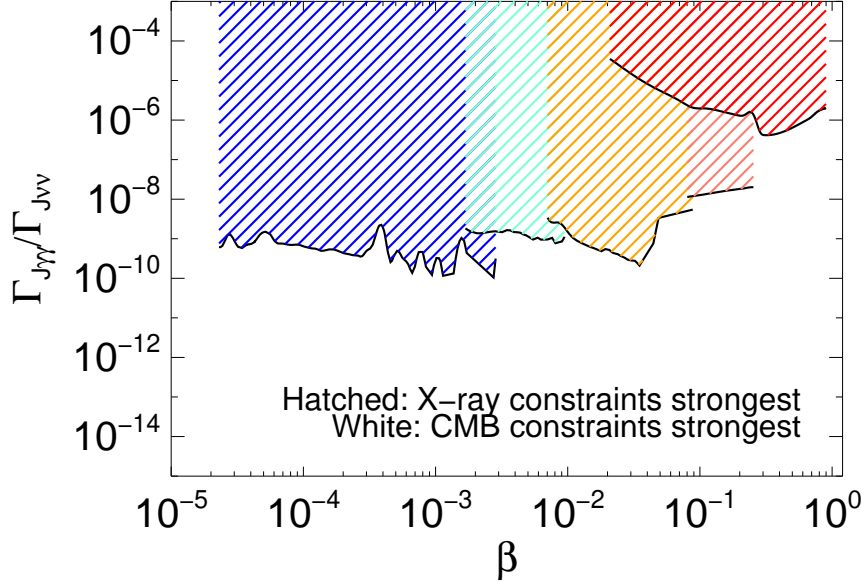


Figure 4. Sensitivity of CMB and x-ray observations to the LDDM majoron scenario as a function of β and $R = \Gamma_J = \Gamma_{J\gamma}$. The black lines are the loci of points where $R = R_*$, i.e., where the CMB and x-ray constraints (from a given object) are equivalent. In the hatched regions above the lines, X-ray constraints are stronger; below, CMB constraints are stronger. The color codes are the same as in Fig. 3. See Sec. 4 for discussion.

constraints, we take the mass of the majoron to be equal to $m_J = 0.145 \text{ keV} = m_{J^*}$, with an associated 1 σ error of $\delta m_J = 0.01 \text{ keV} = \delta m_{J^*}$. Then, we find the maximum Γ_J allowed by the x-ray emission for this value of the mass (as explained in Sec. 3.2). The uncertainty in the exact value of the mass is taken into account by convolving the upper limits shown in Fig. 3 with a Gaussian of mean m_J and variance equal to δm_J^2 . Let us call this value Γ_J^{max} . We also denote with $\Gamma_J^{\text{max}} = 1.3 \times 10^{19} \text{ sec}^{-1}$ the CMB upper limit on the decay width to neutrinos. Then for the following value of the branching ratio:

$$R_* = \frac{\Gamma_J^{\text{max}}}{\Gamma_{J\gamma}^{\text{max}}} \quad (15)$$

the two sets of observations yield exactly the same constraining power. In other words, for this particular value of the branching ratio, it would be the same to constrain the decay rate to photons using the x-rays and then obtain the decay rate to neutrinos using $\Gamma_J = \Gamma_{J\gamma} = R_*$, or to do the contrary, i.e. to use the CMB to constrain the invisible neutrino decay channel and from that obtain a bound on the photon decay. Larger branching ratios ($R > R_*$) will be better constrained by observations of the x-ray emission, while smaller branching ratios ($R < R_*$) will be better constrained by the CMB.

We repeated above procedure for β ranging from 10^{-5} to 1, comparing the x-ray constraints of Fig. 3, one at time, with the CMB constraint. We did not include the

XMM observations of the Milky Way because they are discontinuous and this makes the mass-averaging procedure problematic. The results are illustrated in Fig. 4. We can roughly say that for small majoron masses ($m_J \lesssim 1$), we should resort to x-ray observations to probe the region $R \lesssim 10^6$, while we should use the CMB for $R \gtrsim 10^6$. For large neutrino masses, x-ray observations are better when $R \lesssim 10^8$, while CMB is more informative for $R \gtrsim 10^{10}$.

5. Particle physics

We now turn to the particle physics of our decaying dark matter scenario. Although many attractive options are open [40] possibly the most popular scheme for generating neutrino masses is the seesaw. The simplest type I seesaw model has no induced majoron radiative decays. For this reason we consider the full seesaw model, which contains a Higgs boson triplet coupling to the lepton doublets [41].

In addition to the SM fields one has three electroweak gauge singlet right-handed neutrinos, $\bar{\nu}_{L_i}^c$, a complex $SU(2)_L$ scalar triplet, Δ , with hypercharge 1 and lepton number 2, and a scalar singlet, Φ , with lepton number 2. We will denote the scalar $SU(2)$ doublet as Φ . The Yukawa Lagrangian is given by

$$\begin{aligned} \mathcal{L}_Y = & Y_u \bar{Q}_L^T u_L^c + Y_d \bar{Q}_L^T d_L^c + Y_e \bar{L}_L^T e_L^c \\ & + Y_\Delta \bar{L}_L^T \Delta^c + Y_\Phi \bar{L}_L^T \Phi + \frac{Y_R}{2} \bar{\nu}_L^c \nu_L^c + \text{H.c.} \end{aligned} \quad (16)$$

In order to extract the relevant couplings of the majoron that are responsible for the decays in Eq. (2), we review here the main steps of the procedure developed in [11], using the basic two-component Weyl description of neutrinos as in [41].

Using the invariance of the scalar potential under the hypercharge $U(1)_Y$ and lepton number $U(1)_L$ symmetries and assuming that these are broken spontaneously by the vacuum configuration, one finds, from Noether's theorem, the full structure of the mass matrix of the imaginary neutral component of the scalars given in terms of their vacuum expectation values (vevs) as [11]

$$M^{I2} = \begin{pmatrix} 0 & 4\frac{v_1^2}{v_2^2} & 2\frac{v_1^2}{v_3 v_2} & 2\frac{v_1}{v_2} \\ \frac{B}{C} & 2\frac{v_1^2}{v_3 v_2} & \frac{v_1^2}{v_3} & \frac{v_1}{v_3} \\ \frac{B}{C} & \frac{v_1^2}{v_3} & \frac{v_1}{v_3} & A \\ 2\frac{v_1}{v_2} & \frac{v_1}{v_3} & 1 & 1 \end{pmatrix} \begin{pmatrix} C \\ C \\ A \\ A \end{pmatrix}; \quad (17)$$

with $C = \langle \Phi^2 \rangle V = \langle \Phi^2 \rangle^{-1}$ and v_1, v_2, v_3 are the vevs of the singlet, the doublet, and the triplet, respectively. One sees that M^{I2} has a non zero eigenvalue, $m_A^2 = \text{Tr} M^{I2}$ and two null eigenvalues. These correspond to the Goldstone bosons eaten by the Z gauge boson and, as expected, to the physical Nambu-Goldstone boson associated with the breaking of $U(1)_L$, the majoron J . The parameters of the scalar potential of the model can be chosen so that the pattern of vevs obtained by minimization respects the so-called (type II) seesaw form, namely [11]

$$v_3 \gg v_2 \gg v_1$$

In particular, since the smallness of the triplet vev arises through the vev seesaw relation one can show that it is not spoiled by one-loop radiative corrections.

The resulting profile of the majoron, J , following from Eq. (17) takes a very simple form in this seesaw approximation, namely [11]

$$J = \frac{2v_3^2}{v_1 v_2} \phi_I + \frac{v_3}{v_1} \phi_I + \phi_I; \quad (18)$$

In the presence of the gravitationally induced terms that give mass to the majoron, the mass matrix of Eq. (17) is slightly modified, but these effects are sub-leading and negligible.

We are now ready to determine the coupling of the majoron with the light neutrinos. From Eq. (16) one obtains the full neutrino Majorana mass matrix as

$$M = \frac{1}{2} \begin{pmatrix} Y_L v_3 & Y v_2 \\ Y v_2 & Y_R v_1 \end{pmatrix}; \quad (19)$$

so that the effective light neutrino Majorana mass matrix is given by [11]:

$$M_{LL} = \frac{1}{2} \begin{pmatrix} Y_L v_3 & Y^T Y_R^{-1} Y v_2^2 \\ Y v_2 & Y_R v_1 \end{pmatrix}; \quad (20)$$

The coupling g_J of the majoron to the neutrinos can also be obtained using Noether's theorem according to the procedure described in Ref. [11]. In this way one finds that the majoron couples to the mass eigenstate neutrinos proportionally to their masses,

$$g_{Jrs} = \frac{m_{rs}}{2v_1}; \quad (21)$$

where v_1 describes the scale at which the global lepton number symmetry breaks, typically $10^6 - 10^9$ GeV (see below).

The decay width Γ_J is given by

$$\Gamma_J = \frac{m_J}{32} \frac{(m_r)^2}{4v_1^2}; \quad (22)$$

Let's now turn to g_J . From the Yukawa Lagrangian of Eq. (16) and from Eq. (18) we have that the majoron interacts with the charged fermions through

$$\frac{2v_3^2}{v_2 v_1} Y_f (-2T_{3f}) f_5 f J = \frac{2v_3^2}{v_2^2 v_1} m_f (-2T_{3f}) f_5 f J; \quad (23)$$

where T_{3f} is the weak isospin and we have assumed that the charged fermion mass matrices are diagonal. The interaction term of Eq. (23) gives rise to the interaction term with photons given in Eq. (7), with an effective coupling given by

$$g_J = \frac{1}{2} \sum_f N_f (-2T_{3f}) Q_f^2 + \frac{1}{12} \frac{m_J^2}{m_f^2} \frac{2v_3^2}{v_2^2 v_1}; \quad (24)$$

where one notices the cancellation of the "anomalous-like" contribution $\sum_f N_f (-2T_{3f}) Q_f^2$. As a result we have

$$\Gamma_J = \frac{1}{64} \frac{m_J^3}{\sim 2}; \quad (25)$$

with

$$\sim \frac{1}{f N_f (2T_{3f}) Q_f^2 \frac{1}{12} \frac{m_J^2}{m_f^2}} \frac{v_2^2 v_1}{v_3^2};$$

where Q_f and N_f are the electric charge of f and its colour factor, respectively.

Fig. 5 shows how the currently allowed range of neutrino masses selects an allowed strip in the plane $v_1 - m_J$ consistent with neutrino oscillation data [6] and with the cosmological bounds on neutrino mass [42], assuming that the CMB bound (2) on the $J \rightarrow \gamma\gamma$ decay rate is saturated.

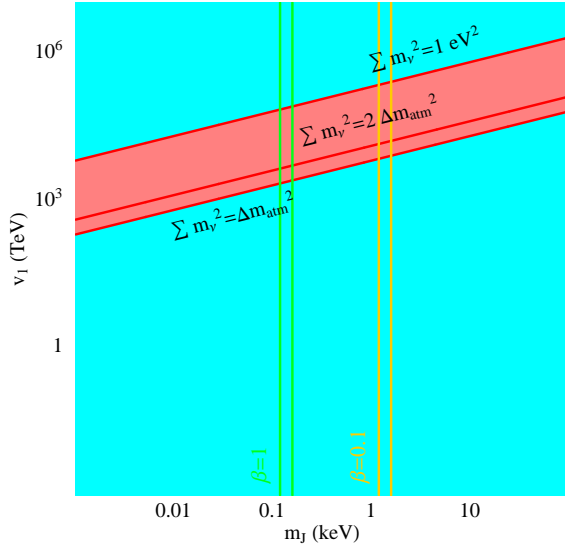


Figure 5. The strip indicates the region in the $v_1 - m_J$ plane allowed by current neutrino oscillation [6] and cosmological data [42], assuming the maximal $J \rightarrow \gamma\gamma$ decay rate. The vertical lines delimit the mass values required by the CMB observations, for different values of β .

The lower lines correspond to the cases of normal and inverse hierarchical neutrino masses, while the top line holds when the three neutrinos are (quasi)-degenerate. The vertical bands in the figure indicate the mass region of Eq. 5 singled out by the CMB observations, for two different values of β .

We also note from Eq. (25) that, for a fixed value of the majoron mass and the lepton number symmetry breaking scale v_1 , the two-photon decay rate only depends on the vev of the triplet and on the sum of the squared masses of the neutrinos, namely on the two possible scenarios in the neutrino sector, hierarchical or degenerate. For a given scenario the decay is then fixed only by v_3 , as it can be seen in Fig. 6, where the top panel corresponds to the hierarchical case while the bottom one holds for the quasi-degenerate spectrum. The diagonal lines in Fig. 6 give the dependence of $\Gamma_{J \rightarrow \gamma\gamma}$ on m_J , for different values of v_3 . As it can also be seen from Eq. (25), the largest values of v_3 correspond to the largest radiative decay rates.

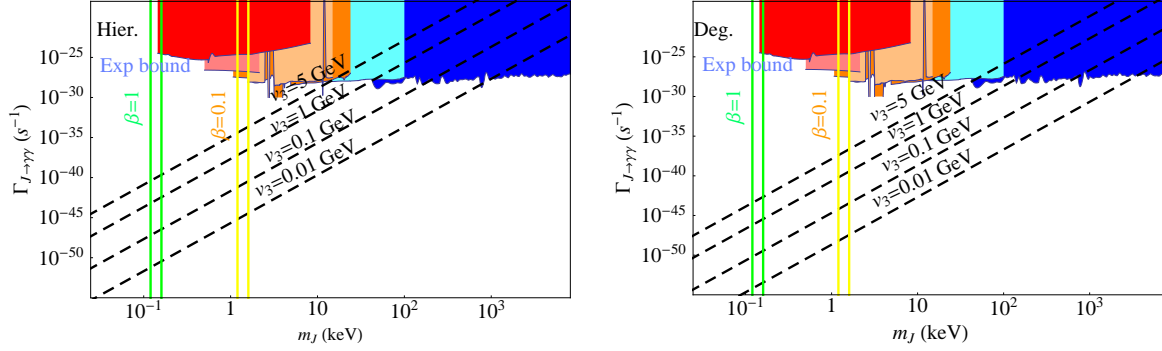


Figure 6. Majoron decay rate to photons as a function of the majoron mass m_J , for different values of the triplet vev, v_3 . We assume the invisible decay bound to be saturated. The top and bottom panels refer to hierarchical and degenerate neutrino mass spectra, respectively. The shaded regions are excluded by observations as described in Sec. 3. The vertical lines are the same as in Fig. 5.

One sees that in both scenarios small m_J and v_3 values lead to decay rates well below the observational bounds. However, for large values of v_3 , say, $v_3 = 5$ GeV, roughly corresponding to the maximum compatible with precision measurements of electroweak parameters [43], the radiative rates fall within the sensitivities of the Milky Way observations displayed in Fig. 3, and would be thereby observationally excluded. For lower masses the observational sensitivities would need to be improved by about 20 orders of magnitude requiring completely new techniques from what is available today. The small radiative majoron decay rates would be avoided in models where the anomaly does not cancel due to the presence of extra fermions. We mention also in this case the possibility of further enhancement due to cumulative effects as those that might arise, for example, in higher dimensions.

6. Summary

We have investigated the production of x-ray photons in the late-decaying dark matter scenario, and quantified the sensitivity of current observations to such a mono-energetic emission line. In particular, we have studied the constraints from the diffuse x-ray observations, as well as by considering the fluxes generated by dark matter dominated objects. These observations provide a probe of radiative dark matter decays and can be used as an "indirect detection" of the LDDM majoron scenario.

We have illustrated this explicitly for the case where neutrinos get mass a la seesaw, where the majoron couples to photons through its Higgs triplet admixture. Alternative particle physics realizations of the LDDM scenario can be envisaged, an issue which will be taken up elsewhere. Let us also mention that Majoron dark matter decays can be possibly probed in the future through 21-cm observations (see Ref. [44] for an application to other DM candidates).

Acknowledgements We thank Antonio Palazzo and Alexei Boyarsky for discussions. This work was supported by MEC grant FPA 2005-01269, by EC Contracts RTN network MRTN-CT-2004-503369 and ILIAS/N6 RII3-CT-2004-506222. The Dark Cosmology Centre is funded by the Danish National Research Foundation. ML is currently supported by INFN.

References

- [1] Super-Kamiokande collaboration, Y. Fukuda et al., Phys. Rev. Lett. 81, 1562 (1998), [hep-ex/9807003].
- [2] SNO collaboration, Q. R. Ahmad et al., Phys. Rev. Lett. 89, 011301 (2002), [nucl-ex/0204008].
- [3] KamLAND collaboration, K. Eguchi et al., Phys. Rev. Lett. 90, 021802 (2003), [hep-ex/0212021].
- [4] KamLAND collaboration, S. Abe et al., 0801.4589.
- [5] MINOS collaboration, arXiv:0708.1495 [hep-ex].
- [6] M. Maltoni, T. Schwetz, M. A. Tortola and J. W. F. Valle, New J. Phys. 6, 122 (2004), arXiv version 6 in hep-ph/0405172 provides updated neutrino oscillation results and references to previous works.
- [7] KATRIN collaboration, G. Drexlin, Nucl. Phys. Proc. Suppl. 145, 263 (2005).
- [8] I. Avignone, Frank T., S. R. Elliott and J. Engel, 0708.1033, a brief summary of the phenomenology of double beta decay can be found in: M. Hirsch, arXiv hep-ph/0609146.
- [9] S. Hannestad, New J. Phys. 6, 108 (2004) [arXiv:hep-ph/0404239]. J. Lesgourgues and S. Pastor, Phys. Rept. 429, 307 (2006), [astro-ph/0603494].
- [10] Y. Chikashige, R. N. Mohapatra and R. D. Peccei, Phys. Lett. B 98, 26 (1981).
- [11] J. Schechter and J. W. F. Valle, Phys. Rev. D 25, 774 (1982).
- [12] S. R. Coleman, Nucl. Phys. B 310, 643 (1988); R. Holman, S. D. H. Hsu, T. W. Kephart, E. W. Kolb, R. Watkins and L. M. Widrow, Phys. Lett. B 282 (1992) 132 [arXiv:hep-ph/9203206]; E. K. Akhmedov, Z. G. Berezhiani and G. Senjanovic, Phys. Rev. Lett. 69 (1992) 3013 [arXiv:hep-ph/9205230].
- [13] V. Berezinsky and J. W. F. Valle, Phys. Lett. B 318 360 (1993) [arXiv:hep-ph/9309214].
- [14] WMAP collaboration, D. N. Spergel et al., Astrophys. J. Suppl. 170, 377 (2007), [astro-ph/0603449].
- [15] M. Lattanzi and J. W. F. Valle, Phys. Rev. Lett. 99, 121301 (2007), [arXiv:0705.2406 [astro-ph]].
- [16] V. Berezinsky, A. S. Joshipura and J. W. F. Valle, Phys. Rev. D 57, 147 (1998) [arXiv:hep-ph/9608307].
- [17] K. Ichiki, M. Oguri and K. Takahashi, Phys. Rev. Lett. 93, 071302 (2004) [arXiv:astro-ph/0403164].
- [18] Y. Gong and X. Chen, arXiv:0802.2296 [astro-ph].
- [19] L. Zhang, X. Chen, M. Kamionkowski, Z. g. Si and Z. Zheng, Phys. Rev. D 76, 061301 (2007) [arXiv:0704.2444 [astro-ph]].
- [20] X. L. Chen and M. Kamionkowski, Phys. Rev. D 70, (2004) 043502 [astro-ph/0310473].
- [21] K. C. Gendreau et al., Publ. Astron. Soc. Jap. 47, L5 (1995).
- [22] D. E. Guber, J. L. Mattheson, L. E. Peterson and G. V. Jung, Astrophys. J. 520, 124 (1999). [arXiv:astro-ph/9903492].
- [23] M. Kawasaki and T. Yanagida, Phys. Lett. B 399, 45 (1997) [arXiv:hep-ph/9701346].
- [24] L. W. Chen, A. C. Fabian and K. C. Gendreau, Mon. Not. R. Astron. Soc. 285, 449 (1997) [arXiv:astro-ph/9511089].
- [25] A. Boyarsky, A. Neronov, O. Ruchayskiy and M. Shaposhnikov, Mon. Not. Roy. Astron. Soc. 370, 213 (2006) [arXiv:astro-ph/0512509].
- [26] A. Boyarsky, A. Neronov, O. Ruchayskiy, M. Shaposhnikov and I. Tkachev, Phys. Rev. Lett. 97, 261302 (2006) [arXiv:astro-ph/0603660].

- [27] A. Boyarsky, J. W. den Herder, A. Neronov and O. Ruchayskiy, *Astropart. Phys.* **28**, 303 (2007) [[arXiv:astro-ph/0612219](#)].
- [28] C. X-ray Centre, 644, L33 (2006) <http://cxc.harvard.edu/proposers/POG/html>
- [29] S. Riemer-Sørensen, S. H. Hansen, K. Pedersen and H. Dahle, *Phys. Rev. D* **76**, 043524 (2007).
- [30] A. Boyarsky, O. Ruchayskiy and M. Markevitch, *Astrophys. J.* **673**, 752 (2008) [[arXiv:astro-ph/0611168](#)].
- [31] A. Fruscione et al. *SP IE Proc.* **6270**, 62701V, D. R. Silva & R. E. Doxsey, eds. (2006). <http://cxc.harvard.edu/ciao/>
- [32] J. F. Navarro, C. S. Frenk and S. D. M. White, *Astrophys. J.* **490**, 493 (1997), [[astro-ph/9611107](#)].
- [33] B. Moore, T. Quinn, F. Governato, J. Stadel and G. Lake, *Mon. Not. Roy. Astron. Soc.* **310**, 1147 (1999)
- [34] M. C. Bentz, B. M. Peterson, R. W. Pogge, M. Vestergaard and C. A. Onken, *Astrophys. J.* **644**, 133 (2006), [[astro-ph/0602412](#)].
- [35] A. Boyarsky, J. Nevalainen and O. Ruchayskiy, *Astron. Astrophys.* **471**, 51 (2007) [[arXiv:astro-ph/0610961](#)].
- [36] C. R. Watson, J. F. Beacom, H. Yuksel and T. P. Walker, *Phys. Rev. D* **74**, 033009 (2006) [[arXiv:astro-ph/0605424](#)].
- [37] A. Boyarsky, D. Iakubovskyi, O. Ruchayskiy and V. Savchenko, [arXiv:0709.2301 \[astro-ph\]](#).
- [38] H. Yuksel, J. F. Beacom and C. R. Watson, [arXiv:0706.4084 \[astro-ph\]](#).
- [39] A. Boyarsky, D. Malyshev, A. Neronov and O. Ruchayskiy, [arXiv:0710.4922 \[astro-ph\]](#).
- [40] H. Nunokawa, S. J. Parke and J. W. F. Valle, *Prog. Part. Nucl. Phys.* **60**, 338 (2008), [[arXiv:0710.0554 \[hep-ph\]](#)].
- [41] J. Schechter and J. W. F. Valle, *Phys. Rev. D* **22**, 2227 (1980).
- [42] J. Dunkley et al. [WMAP Collaboration], [arXiv:0803.0586 \[astro-ph\]](#).
- [43] Particle Data Group, W. M. Yao et al., *J. Phys. G* **33**, 1 (2006).
- [44] M. Valdes, A. Ferrara, M. M. Apelli and E. Ripamonti, *Mon. Not. Roy. Astron. Soc.* **377**, 245 (2007) [[arXiv:astro-ph/0701301](#)].